Electrical Power and Energy Systems 118 (2020) 105756

Contents lists available at ScienceDirect

Electrical Power and Energy Systems

journal homepage: www.elsevier.com/locate/ijepes

Protection of microgrids using voltage-based power differential and sensitivity analysis

Patrick T. Manditereza[a,*], Ramesh C. Bansal[b]

[a] Department of Electrical, Electronic and Computer Engineering, Central University of Technology, Free State, South Africa
[b] Department of Electrical Engineering, University of Sharjah, Sharjah, United Arab Emirates

ARTICLE INFO

Keywords:
Microgrid protection
Protection performance
Distributed energy resources
Distribution system protection
Distributed algorithms
Fault detection indices

ABSTRACT

Microgrids are emerging as an alternative mode of operation for distribution systems integrated with Distributed Energy Resources (DERs). With appropriate management and control of the DERs, a section of a distribution system can operate isolated from the main grid thereby enhancing the reliability and security of supply to consumers. However, the integration of DERs has raised many technical challenges including protection. The traditional distribution system protection cannot provide reliable protection to the microgrid in the isolated mode due to the limited short-circuit capacities of the converter-interfaced DERs. This paper proposes the application of a new voltage-based relay type for the protection of microgrids. The relay algorithm achieves its protection function through active power differential and sensitivity calculations based on voltage measurements within a specified protection zone. In the paper, the new relay type is modelled in Digsilent PowerFactory software and installed at the nodes of a microgrid test system. The performance of the relay type is investigated under variety of faults. The relay is shown to operate correctly and effectively to detect and identify faults in both radial and meshed microgrids integrated with inverter-interfaced DER technologies.

1. Introduction

Policies being enacted by governments worldwide towards reducing greenhouse effects have influenced a shift towards clean energy sources [1]. This has seen an increasing number of distributed energy resources (DERs) based on renewable sources being integrated into the power grid. The DERs are relatively small and numerous compared to the traditional generating sources, and are dispersed according to resource availability. This is leading to fundamental changes to the topology and characteristics of the electric power system, especially at the distribution level [2,3]. With the penetration of DERs, microgrids are emerging as an alternative mode of operation for distribution systems where a section of a distribution system can operate isolated from the main grid [4]. With appropriate management and control, the DERs in the isolated system can supply the connected loads thereby creating an autonomous distribution system, or microgrid. This mode of operation allows the microgrid to provide reliable and secure energy supply to the local consumers in the event of grid faults [4]. Excess local generation can also be exported back to the grid and support quick recovery of the grid following fault. Microgrids also provide a flexible architecture for the supply of reliable and secure energy to rural communities that are remote from the national grid [5].

However, the integration of DERs has raised many technical challenges including protection. It has been shown [6] that system protection at the distribution level is compromised when a significant amount of DER units are integrated into the power system, leading to possible loss of coordination of the traditional protection that may significantly impact the reliability of the distribution system. The protection problem is exacerbated when the distribution system operates in the microgrid mode. The traditional distribution protection cannot provide reliable protection to the microgrid due to the limited short-circuit capacities of the converter-interfaced DERs in the microgrids [4]. The growing penetration of DERs, therefore, makes microgrid protection an important research topic on the future of power systems.

Notwithstanding the on-going research and published work on microgrid protection, a dedicated and effective microgrid protection system has not been achieved [4]. This has seen protection systems traditionally found on the transmission and sub-transmission systems, such as directional overcurrent relays (DOCR), distance and differential relays being proposed for use on the microgrid.

Zarei et al. [7] have proposed a comprehensive protection strategy that uses different protection relay types for the different elements of the microgrid. These include DOCR, directional negative sequence current and differential protection. The various protection elements are

* Corresponding author.
E-mail address: pmandite@cut.ac.za (P.T. Manditereza).

https://doi.org/10.1016/j.ijepes.2019.105756
Received 19 August 2019; Received in revised form 29 November 2019; Accepted 1 December 2019

employed in a coordinated manner. However, Hooshyar et al. [4] have presented a comprehensive analysis of the performance of traditional protection systems when applied to the microgrid and found that the difference between the fault characteristics of microgrids and transmission systems impact the performance of DOCR, distance and differential relays. An additional drawback of differential relays is the considerably higher cost. The work reported in [8,9] propose new types of directional elements that are not affected by the fault behavior of the DER units and help improve performance of the DOCR.

Due to the difference in sensitivity requirements, some researchers [10,11] have proposed dual-strategy protection schemes for the microgrid, with one strategy for grid-connected mode and the other for islanded mode. In addition to sensitivity requirements, the protection strategies are also influenced by the topology of the microgrid, whether radial or looped [10,12,13].

Communication networks are expected to play a critical role in microgrid protection systems [11]. Communication facilitates the application of protection systems such as distance and differential relaying. The DOCR relays, when applied to the microgrid, may need to adapt their tripping currents due to the varying nature of the DER outputs. Researchers in [14] have proposed a communication assisted dual setting DOCR protection scheme for micro-grids with grid connected and islanded capability. Optimal settings are calculated and proper coordination is maintained with the aid of communication. The work reported in [15] overcomes the overcurrent selectivity problems by using selectivity mechanisms that are supported by agent-based distributed communication. In [9], an adaptive directional overcurrent relaying technique based on the positive-sequence (PSQ) and negative-sequence (NSQ) superimposed currents is proposed.

The methods that do not require physical communications are reported in the literature [12,16]. The authors in [12] proposed a method for microgrids with looped configuration that employs simple overcurrent relays with inverse time-current characteristics. The relays have the same pick-up and time multiplier settings. Following a fault in the microgrid the inverter control at each DER acts to contribute current to the fault that is proportional to the microgrid impedance measured at that location. Selectivity is achieved by the DER closest to the fault contributing a relatively larger current. In [16] inverter control is manipulated to limit the fault current to acceptable limits but also injects a percentage of fifth harmonic to the fault current. The Fast Fourier Transform (FFT) is used to extract the harmonic currents and facilitate identification of the fault. Droop control based on the current-fault resistance characteristic is also employed to make the inverter closer to the fault inject larger current to the fault and achieve selectivity by inverse-time current principle.

The authors in [17,18] have presented an argument for the decoupling of protection strategies from inverter control and shift towards voltage-based protection strategies. Using voltage-based protection, the fault current contribution from the DERs may not be required to achieve effective protection. Various voltage-based protection methods are reported in the literature. Voltage Total Harmonic Distortion (THD) has been identified as a feature that can be used for fault detection. Protection schemes presented in [7,19] use the THD content of the voltage for the identification and location of fault in networks with inverter interfaced DERs. The THD arises due to the inverter controller limiting the current to 1.2–2 times the nominal current. The limiter saturates under fault conditions resulting in the generation of distorted voltages and currents. Researchers in [20,21] use Park's (abc-dq) transformations on the measured system voltages to detect faults through disturbances they cause to the d-q values.

This paper proposes an algorithm that achieves its protection function through active power differential and sensitivity calculations based on synchronized voltage phasor measurements within a specified protection zone. Some sensitivity-based fault detection indices (FD-Indices) were identified that are generated when a fault occurs within a protection zone. The proposed relay type has the potential to overcome the challenges of protecting the microgrid in various ways:

a. The performance of the relay algorithm is independent of the DER technology, whether inverter interfaced or directly coupled to the grid,
b. The algorithm implements a form of distributed protection, meaning that information exchange is limited between relays or intelligent electronic devices (IEDs) located at neighbouring nodes, not network wide,
c. The algorithm is independent of the topology of the network,
d. The possible configuration of the microgrid does not need to be predefined before implementation of the protection. The algorithm is reconfigurable depending on the number of feeders terminating at a node, and
e. The algorithm is instantaneous in operation which allows fast voltage recovery to facilitate fault ride through capability of the DERs and improved microgrid stability.

The rest of this paper is organized as follows: Application of the new relay type is introduced in Section 2. The microgrid adopted for the study is described in Section 3, after which the algorithm of the new relay type and its application to the microgrid is discussed in Section 4. The modelling of the new relay type in Digsilent *Powerfactory* is described in Section 5. The performance of the relay when applied to the microgrid is demonstrated and discussed in Section 6. Conclusions are drawn in Section 7.

2. Phasor measurement technology

The use of Wide Area Measurement Systems (WAMS) is expanding in the electric power industry for improved monitoring, supervision, control and protection of power networks [22,23]. These services are facilitated by the deployment of Phasor Measurement Units (PMUs) that measure the magnitude, phase angle and frequency of the voltage and current signals. Real-time visualization of the power network can then be obtained for fast detection of disturbances.

Reliable communication systems need to be concurrently deployed in order for the various components of the WAMS to interact. Communication technologies and networks have been developed that provide bandwidth sufficient to offer the services required for the monitoring, control, operation and protection of power networks including microgrids [24]. Various physical communication links, including fibre-optic communication, have been proposed in the literature and tested for suitability to microgrid application [25,26]. Fibre-optic communication, in particular, is reliable and provides high-speed protection. The protection system proposed in this paper assumes the availability of high-speed physical communication links along the feeders to minimize communication latency and improve performance of the protection algorithm.

2.1. Proposed protection algorithm application

The protection algorithm proposed in this paper uses PMU data transferred over a suitable communication channel. Basically, the proposed protection algorithm detects fault through active power differential and sensitivity calculations over a defined protection zone. The protection zone, referred to as the Busbar Area Protection (BAP) zone, comprises a busbar and all feeders terminating at that node [3]. The algorithm requires, as inputs, the synchronized measurements of the fundamental voltage magnitude and phase at the 'home' node k (where the relay is located) and at the nodes at the remote ends of the feeders, as illustrated in Fig. 1 for a BAP zone comprising busbar 2 and its three feeders. The algorithm can detect a fault anywhere within the BAP zone; that is, on Line12, Line23, Line24, or on the busbar itself. However, peer-to-peer communication is required, as explained in Section 4.5, for identification of the actual faulted feeder within this zone.

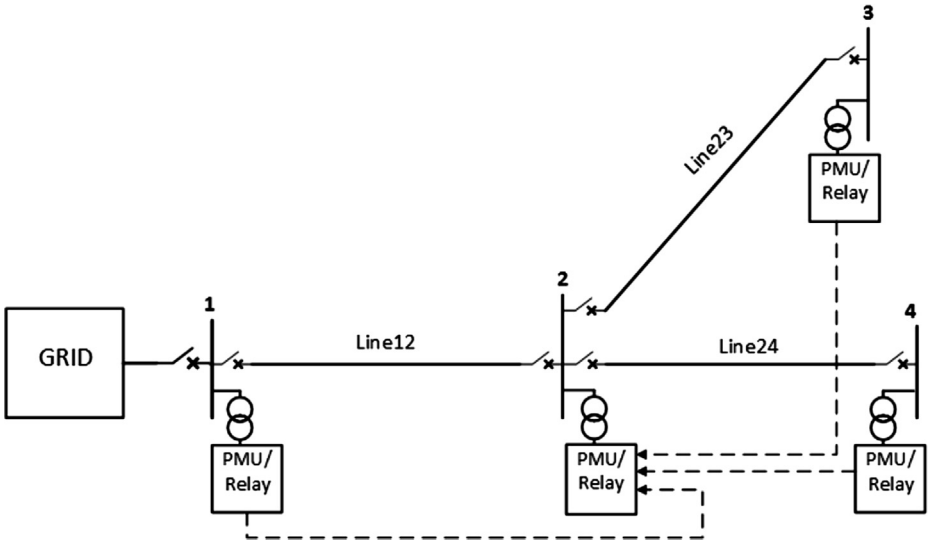

Fig. 1. Proposed protection algorithm application.

A phasor measurement unit (PMU) built into the IED/relay, or separate, needs to be installed at each node in order for the voltage phasors to be made available to the IED. The PMUs provide time-synchronized measurements of the node voltages in real time [27]. The synchronization is achieved by using timing signals received from an accurate source such as the global positioning system (GPS). Data on the simultaneously sampled voltages are then transferred to neighbouring PMUs/IEDs through peer-to-peer communications.

The work reported in [28] has shown that it is possible to configure (n-1) PMUs to operate as servers and stream data to one client PMU on which a control algorithm is deployed, as illustrated in Fig. 1. PMUs have several communication ports that can be configured to receive or transmit data through a specific communication protocol. Usually the PMUs operate in server mode and stream synchrophasor measurements to a phasor data concentrator (PDC) operating in client mode. The work in [28] modified this approach to allow several PMUs to stream data to one PMU, showing that direct communications can be implemented between PMUs for the sharing of synchro-phasor data, thus eliminating the requirement of an intermediate PDC. The synchrophasor measurements can then be utilized internally by the PMU/IED to deploy the protection function. Various protection and control schemes using this synchrophasor transfer approach are reported in [29,30].

Today, PMUs and synchrophasors are generally used for observation of the transmission grid. Application on the distribution network has been limited due to technical and economic barriers [31]. However, due to the integration of DERs there is growing need to ensure security of supply at the distribution level. This requires the deployment of sensors such as PMUs. Observation of the distribution system requires PMUs with higher measurement precision. In transmission systems, because of the large X/R ratio, real and reactive power flows can be mathematically decoupled and real power flow can be assumed to vary mainly with phase angle difference, δ. Large phase differences are thus encountered on the transmission system between two nodes. However, due to the low X/R ratio on the distribution system, the decoupling is not efficient and real power flow depends on both voltage magnitude and phase angle differences. Coupled with the shorter distances on the distribution network, the phase angle differences are much smaller between two nodes compared with those on the transmission system. The PMUs used on the distribution system should therefore have the ability to measure the very small phase angle separations. Micro-phasor measurement units (μPMUs) with higher precision are now economically feasible and available for use on the distribution system and their performance were demonstrated by the work reported in [31–33].

A most interesting and economically important feature of the protection proposed in this paper is that only one relay is required at a node/busbar irrespective of the number of feeders terminating at the node, as illustrated in Fig. 1. This contrasts with most other protection relaying systems, for example directional overcurrent protection, that require at least one relay dedicated to each feeder. This aspect, combined with the emergence of technically and economically viable μPMU technologies, promises to make voltage phasor based protection a viable option.

2.2. Measurement and communication latency

The protection scheme based on the proposed algorithm integrates the PMU measurement technology, the communication link, and the IED running the protection algorithm. There are therefore inherent latencies arising from the measurement reporting delays, the propagation delay of the physical layer medium and the processing time of the algorithm. The IED thus receives the local PMU data earlier than the data from the remote PMUs which delays the fault detection. It is necessary that the latency be characterised for correct evaluation of the relay trip time following fault occurrence. Researchers in [34] developed a method for accurately determining the end-to-end reporting latency of the PMU and the associated propagation and processing delays. The work reported a relay trip time of less than 60 ms from fault inception for a current differential scheme employing PMU data transferred over a WAN. However, latency was not represented in the simulation studies reported in this paper. The proposed algorithm is 'differential' in principle and sees fault in its BAP zone only and works under a similar environment to that in [34] the only difference being the actual algorithm. The equations of the algorithm are not complex and the relay operating time will be similar to that reported in [34]. No intentional time delays for grading purposes are necessary.

3. Adopted test microgrid

The CIGRE Task Force (TF) C6.04.02 developed test systems to facilitate the analysis of DER integration at high voltage, medium voltage, and low voltage levels [35]. The CIGRE benchmark medium voltage (MV) network with the topology shown in Fig. 2 has been selected for the study. This network is derived from a real MV network supplying a small town and its neighbouring rural area. The rated voltage has been adapted to 22 kV at 50 Hz.

The network may operate as two independent radial microgrids if

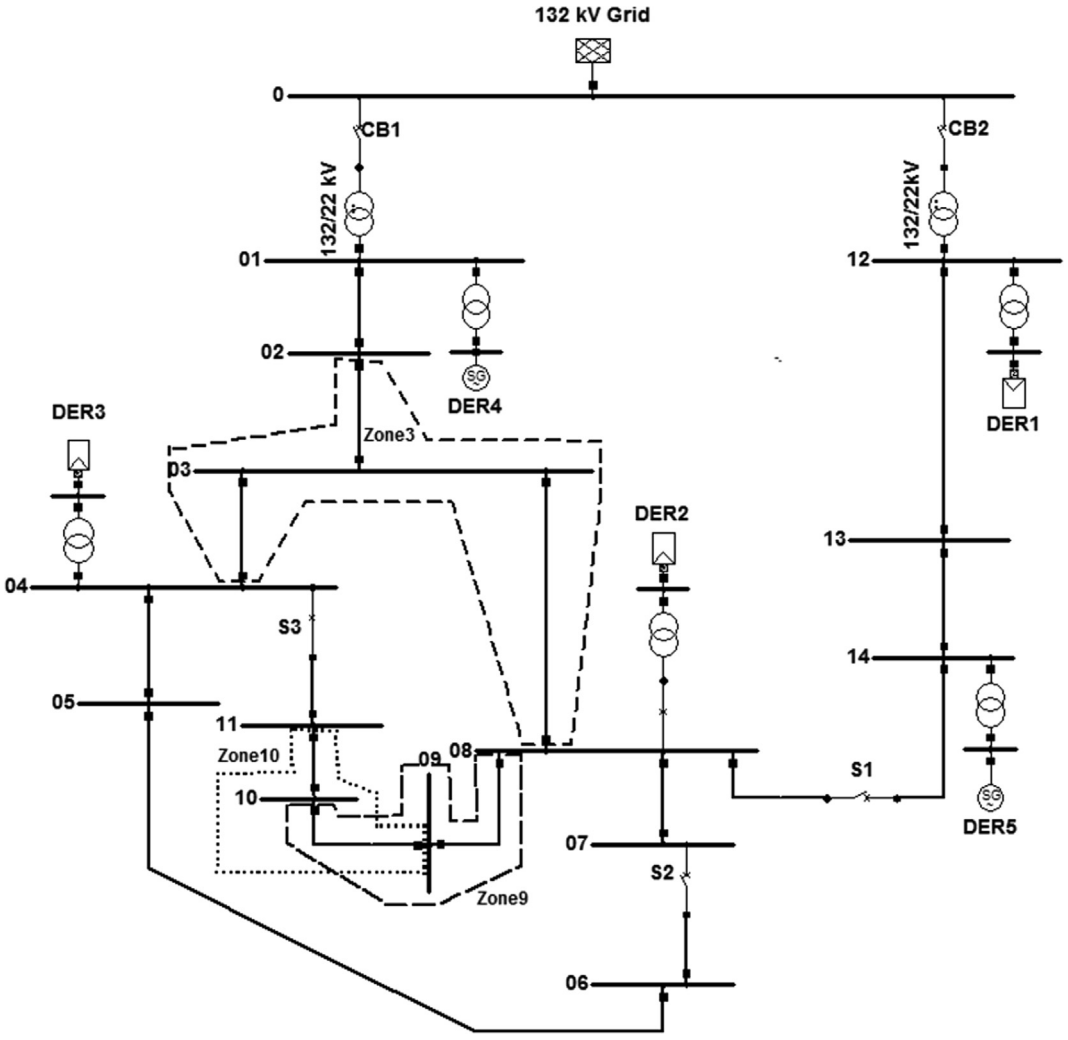

Fig. 2. CIGRE benchmark MV test network.

the circuit breakers CB1 and CB2 that connect the network to the grid are opened. Meshed topologies can be obtained by closing the switches S1, S2 and S3. The network data can be found in [35]. Distributed generators are added to the microgrid including three Photovoltaic (PV) plants at nodes 4, 8 and 12, respectively, as shown in Fig. 2. The generation at node 4 is 18 MW, and 15 MW at each of nodes 8 and 12. Two synchronously coupled generators are connected at nodes 1 and 14. The total capacity of the distributed generators is sufficient to supply the residential and commercial/industrial loads in the network. PV system models available in Digsilent PowerFactory were used for the simulations. The fault current contribution of the PV systems is limited to full load current of 1.0 p.u.

4. Proposed protection algorithm

4.1. Power-voltage sensitivity analysis

The power flow at busbar k of an N-node network can be expressed as [36]:

$$\begin{cases} P_k = \sum_{j=1}^{N} V_k V_j Y_{kj} cos(\delta_k - \delta_j - \delta_{kj}) \\ Q_k = \sum_{j=1}^{N} V_k V_j Y_{kj} sin(\delta_k - \delta_j - \delta_{kj}) \end{cases} \quad (1)$$

where P_k, Q_k, V_k, and δ_k are the active power, reactive power, voltage magnitude and angle at node k; Y_{kj} and δ_{kj} are the magnitude and argument of the element (k, j) in the network's admittance matrix.

The transfer admittance Y_{kj} is zero if no direct connection exists between nodes k and j. Thus, for a BAP segment with n nodes, and the nodes re-numbered from 1 to n, the load flow at node k can be expressed as:

$$\begin{cases} P_k = V_k^2 Y_{kk} cos(-\delta_{kk}) + \sum_{\substack{j=1 \\ j \neq k}}^{n} V_k V_j Y_{kj} cos(\delta_k - \delta_j - \delta_{kj}) \\ Q_k = V_k^2 Y_{kk} sin(-\delta_{kk}) + \sum_{\substack{j=1 \\ j \neq k}}^{n} V_k V_j Y_{kj} sin(\delta_k - \delta_j - \delta_{kj}) \end{cases} \quad (2)$$

The sensitivity of P and Q to bus voltage changes may be expressed using the Jacobian matrix:

$$\begin{bmatrix} \Delta P \\ \Delta Q \end{bmatrix} = \begin{bmatrix} \frac{\partial P}{\partial \delta} & \frac{\partial P}{\partial V} \\ \frac{\partial Q}{\partial \delta} & \frac{\partial Q}{\partial V} \end{bmatrix} \cdot \begin{bmatrix} \Delta \delta \\ \Delta V \end{bmatrix} \quad (3)$$

As already discussed, the proposed protection algorithm achieves its protection function through power differential and sensitivity calculations over a defined BAP zone. Three of these BAP zones, Zone-3, Zone-9 and Zone-10, are shown in the test network of Fig. 2. From (3), the change in P and Q at node k for an n-node BAP segment, may be expressed as:

$$\Delta P_k = \frac{\partial P_k}{\partial \delta_k} \Delta \delta_k + \sum_{\substack{j=1 \\ j \neq k}}^{n} \frac{\partial P_k}{\partial \delta_j} \Delta \delta_j + \frac{\partial P_k}{\partial V_k} \Delta V_k + \sum_{\substack{j=1 \\ j \neq k}}^{n} \frac{\partial P_k}{\partial V_j} \Delta V_j \quad (4)$$

$$\Delta Q_k = \frac{\partial Q_k}{\partial \delta_k}\Delta\delta_k + \sum_{\substack{j=1 \\ j\neq k}}^{n} \frac{\partial Q_k}{\partial \delta_j}\Delta\delta_j + \frac{\partial Q_k}{\partial V_k}\Delta V_k + \sum_{\substack{j=1 \\ j\neq k}}^{n} \frac{\partial Q_k}{\partial V_j}\Delta V_j \quad (5)$$

From (4) and (5), the voltage (magnitude) deviation at node k is given by:

$$\Delta V_k = M^{-1}[(N^{-1}(\Delta P_k - R)) - (T^{-1}(\Delta Q_k - U))] \quad (6)$$

where,

$$M = \left[\left(\frac{\partial P_k}{\partial \delta_k}\right)^{-1}\left(\frac{\partial P_k}{\partial V_k}\right) - \left(\frac{\partial Q_k}{\partial \delta_k}\right)^{-1}\left(\frac{\partial Q_k}{\partial V_k}\right)\right]$$

$$N = \frac{\partial P_k}{\partial \delta_k}$$

$$T = \frac{\partial Q_k}{\partial \delta_k}$$

$$R = \left(\sum_{\substack{j=1 \\ j\neq k}}^{n} \frac{\partial P_k}{\partial \delta_j}\Delta\delta_j + \sum_{\substack{j=1 \\ j\neq k}}^{n} \frac{\partial P_k}{\partial V_j}\Delta V_j\right)$$

$$U = \left(\sum_{\substack{j=1 \\ j\neq k}}^{n} \frac{\partial Q_k}{\partial \delta_j}\Delta\delta_j + \sum_{\substack{j=1 \\ j\neq k}}^{n} \frac{\partial Q_k}{\partial V_j}\Delta V_j\right)$$

Eq. (6) can then be written as,

$$\Delta V_k = S_{V,P}.\ \Delta P_k + S_{V,Q}.\ \Delta Q_k + V_{D,k} \quad (7)$$

where,

$$S_{V,P} = M^{-1}N^{-1}$$

$$S_{V,Q} = -M^{-1}T^{-1}$$

$$V_{D,k} = -(M^{-1}N^{-1}R - M^{-1}T^{-1}U)$$

From (7),

$$\Delta Q_k = -\left(\frac{S_{V,P}.\ \Delta P_k}{S_{V,Q}} - \frac{\Delta V_k - V_{D,k}}{S_{V,Q}}\right) \quad (8)$$

Eq. (8) may be written as,

$$\Delta Q_k = C_{k,P} - C_{k,V} \quad (9)$$

where,

$$C_{k,V} = -\left(\frac{\Delta V_k - V_{D,k}}{S_{V,Q}}\right) \quad (10)$$

$$C_{k,P} = -\left(\frac{S_{V,P}.}{S_{V,Q}}\right)\Delta P_k \quad (11)$$

Element-wise multiplication of (10) and (11) gives,

$$C_{k,F} = \left(\frac{\Delta V_k - V_{D,k}}{S_{V,Q}}\right)\left(\frac{S_{V,P}.}{S_{V,Q}}\right)\Delta P_k \quad (12)$$

Eqs. (11) and (12) give the fault detection indices (FD-Indices) $C_{k,P}$ and $C_{k,F}$ on which the protection algorithm proposed in this paper is based. The algorithm is sensitive to real (active) power flow changes (ΔP_k) only and assumes resistive fault impedance.

4.2. Fault detection principle

The fault detection principle is introduced by considering the case where a resistive load connected at node k changes by magnitude ΔP_k. It can be deduced from (8) that under steady state conditions (i.e. with constant load magnitude),

$$\Delta V_k = V_{D,k} \quad (13)$$

since $\Delta Q_k = \Delta P_k = 0$.

The change of load by magnitude ΔP_k causes generation of the quantity $C_{k,P}$ at node k, according to (11). The node voltage also changes by magnitude ΔV_k causing the quantity $V_{D,k}$ to shift away from ΔV_k in order to generate, according to (9) and (10), the equal and opposite quantity $C_{k,V}$, thus maintaining $\Delta Q_k = 0$ at that node, since the load does not draw reactive power from the system (the connected load is purely resistive). The magnitude of this deviation ($\Delta V_k - V_{D,k}$) depends on the magnitude of ΔP_k. $V_{D,k}$ can be defined from (7) as a (voltage) variable whose magnitude depends on the sensitivity of the voltages at all nodes in the BAP segment to changes in active power at node k. Thus, $V_{D,k}$ is effectively a parameter that monitors the power flow conditions across each BAP segment. The result of this monitoring is such that $\Delta V_k = V_{D,k}$ when there is no 'leakage' or sudden load change within the segment.

A short circuit to ground through a resistive fault impedance drives power equivalent to $I_F^2 R_F$ to ground through a 'leakage' or fault path, where I_F is the fault current and R_F is the fault resistance, causing power flow imbalance across the BAP zone. This is equivalent to sudden connection of a load at the node, or the fault is seen as such by the algorithm, and will have the same effect, generating the quantity $C_{k,P}$. The fault causes voltage drop ΔV_k at node k. The magnitudes and phase angles of the voltages at the other nodes in the protection zone also change causing $V_{D,k}$ to change as well. A new operating point is quickly established. The total effect is to cause a difference between ΔV_k and $V_{D,k}$ which generates the FD-Indice $C_{k,F}$, according to (12). The operation of the fault detection algorithm can thus be described as:

$\Delta V_k = V_{D,k}$, balanced conditions; no fault in protection zone of node k

$\Delta V_k \neq V_{D,k}$, unbalanced conditions; indicates fault in protection zone of node k

The proposed algorithm detects fault at the transition from pre-fault to post-fault condition illustrated in Fig. 3. The pre-fault voltage phasor 'frame' is compared with the post-fault 'frame' which, in the event of fault, causes the generation of the quantities ΔV_k, $V_{D,k}$, and the FD-Indices $C_{k,P}$and $C_{k,F}$. The process of generating the FD-Indices from the received voltage phasors is illustrated in Fig. 4 for a 3-node line segment. ΔV_k is calculated from the base case (or pre-fault) value of voltage at node k, V_k^0, stored in memory, and the real time (post-fault) value, V_k^1. The current (post-fault) and base case magnitudes and phase angles of the voltages at all the nodes in the segment are required for the calculation of $V_{D,k}$, according to (6) and (7). The two quantities, ΔV_k and $V_{D,k}$, are then used to generate $C_{k,V}$ according to (10). The figure extends to show the generation of $C_{k,P}$. $C_{k,F}$ is derived from the element-wise multiplication of $C_{k,P}$ and $C_{k,V}$. FD-indices above pick-up threshold assert the fault detection and identification (FDI) flag.

The above discussion focused on faults involving ground. However, the same results are obtained for phase-to-phase faults that may not involve ground. In this case also, the power into the protection zone is

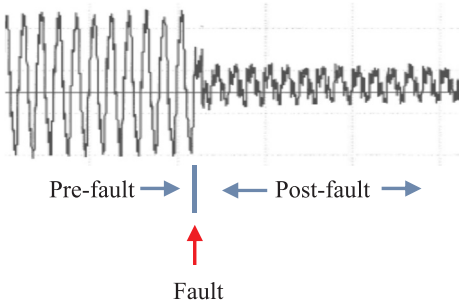

Fig. 3. Typical voltage waveform pre- and post-fault.

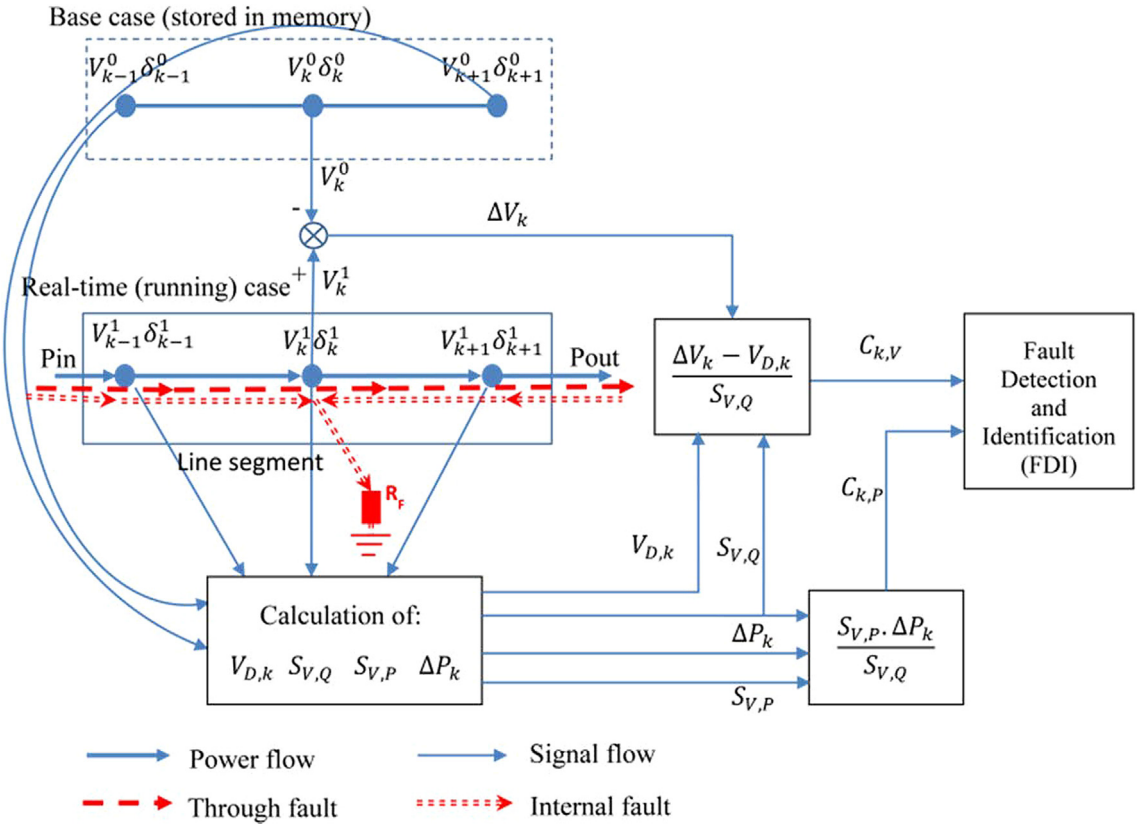

Fig. 4. Power flow balance across a 3-node line segment under fault conditions.

not equal to that exiting the zone causing the unbalanced condition ($\Delta V_k \neq V_{D,k}$) that indicates fault.

From (9) it is apparent that the quantities $C_{k,V}$ and $C_{k,P}$ have units of p.u. [MVAr]. In essence, $C_{k,V}$ and $C_{k,P}$, and hence $C_{k,F}$, are MVAr-based quantities (or indices) that are generated when differential power due to fault or load is detected. It is shown in this paper that the $C_{k,P}$ and $C_{k,F}$ indices due to short circuits are several orders of magnitude higher than those due to connection of load, and can be used for the detection of short circuit fault.

The above analysis shows that it is possible to detect short circuits through simple power differential and sensitivity calculations based on voltage measurements only. It is, thus, not necessary to calculate or know the fault current or the fault contribution of the multiple generators integrated into a power network.

An important attribute of the proposed protection method is that it is independent of the topology of the electrical network. As discussed above, the algorithm performs power differential and sensitivity calculations at each node using the voltage phasor measurements at the 'home' node (k) and neighbouring nodes in the BAP zone only. The protection thus does not see the structure of the network beyond the neighbouring node(s). This is important in two respects:

(a) The complexity of the network beyond the BAP zone is not apparent to the algorithm. The protection zoning arrangement splits the network into overlapping sections each comprising a busbar and the feeders terminating at that node. It does not matter if the network is radial or meshed.
(b) Knowledge of the power sources (type, size or locations) is not important since the algorithm only monitors power flows across a BAP zone, i.e. the protection does not need information about the source of the power flow or where these sources are located.

4.3. Relay functionality

The FD-Indices are calculated at each node of the network. The calculations are performed for each phase, for all three phases. This means that each relay at a node should have three fault detection elements, one for each phase. The faulted phase is indicated by operation of the respective relay element. A phase-to-phase fault is indicated by operation of the respective relay elements that monitor the two phases. A detailed functional description of the fault detection process is given in Fig. 5. Using PMUs, the IED running this algorithm takes the synchronized voltage measurements from the local and neighbouring nodes as inputs. Basically, the current (real-time) 'frame' of phasor values received from the PMUs, and pre-fault 'frame' of phasors stored in memory are read into the algorithm and the fault detection calculations performed. FD-Indices are generated and a fault is indicated when FD-Indices above the threshold are detected.

4.4. Network reconfiguration

Application of the proposed algorithm requires knowledge of the microgrid network model. For example, the admittance matrix of a BAP segment needs to be updated when a line is disconnected from a busbar. Eq. (14) shows the expression for the calculation of one of the sensitivity terms, $\frac{\partial P_2}{\partial V_2}$, at node 2 of a 4-node BAP segment [36].

$$\frac{\partial P_2}{\partial V_2} = V_1 Y_{21}\cos(\delta_2 - \delta_1 - \delta_{21}) + 2V_2 Y_{22}\cos(-\delta_{22}) + V_3 Y_{23}\cos(\delta_2 - \delta_3 - \delta_{23}) + V_4 Y_{24}\cos(\delta_2 - \delta_4 - \delta_{24}) \quad (14)$$

where V_n and δ_n ($n = 1, 2, 3, 4$) are respectively the voltage magnitude and angle at node n; Y_{kj} and δ_{kj} are respectively the magnitude and argument of the element (k, j) in the BAP segment's admittance matrix ($k = 2; j = 1, 3, 4$).

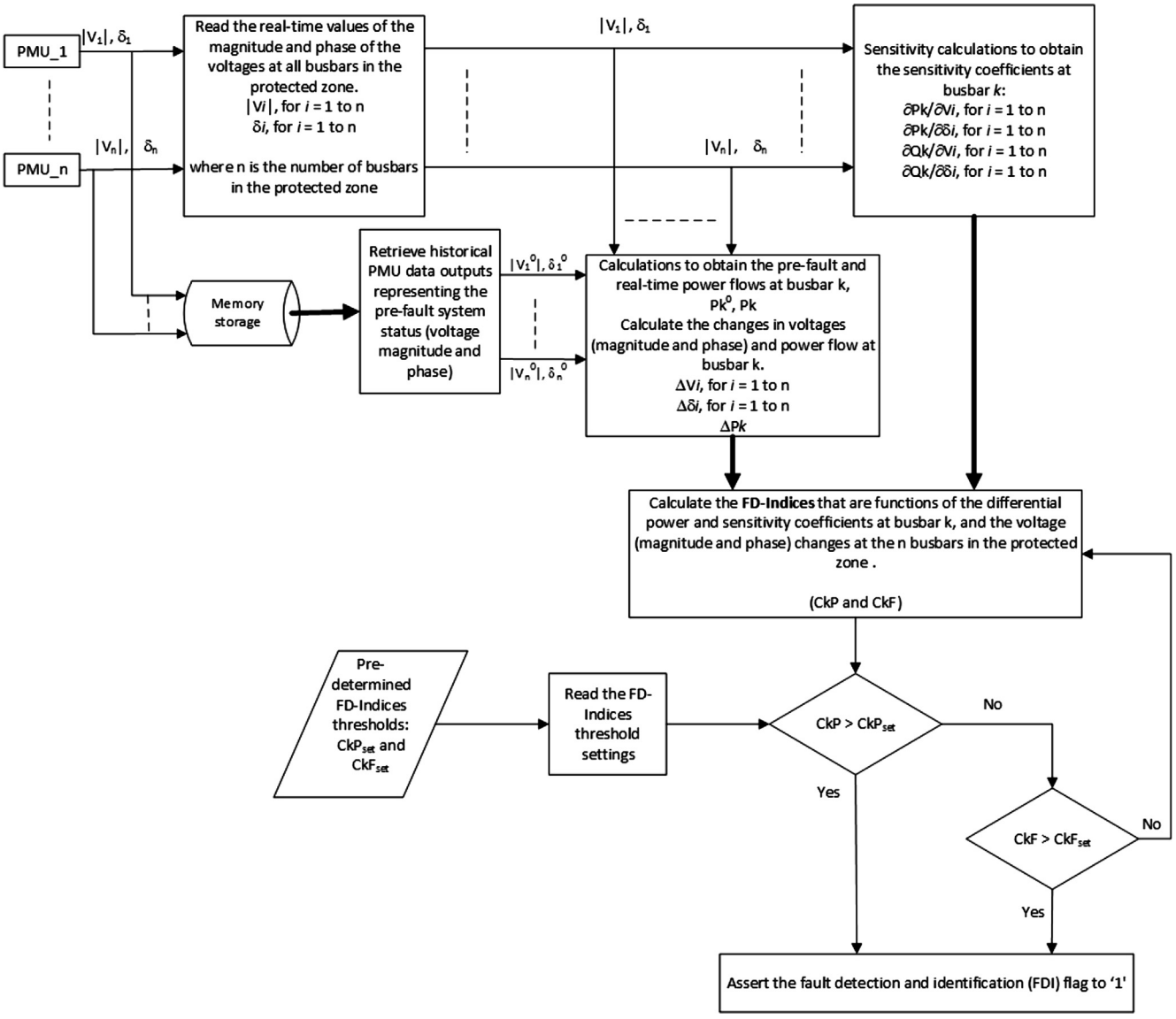

Fig. 5. Detailed functional description of fault detection process.

If Line24 of Fig. 1, for example is taken out of service, the last term of (14) needs to be removed from the expression. The self-admittance Y_{22} also needs to be adjusted. However, this problem can be addressed by making use of settings groups to deal with line outages following fault or for maintenance purposes. Each IED at a node should therefore revert to a particular settings group depending on the status or availability of the feeders that terminate at that node. This makes the algorithm reconfigurable in order to match the number of feeders terminating at node k and still function correctly.

In essence, the protection relay at busbar 2 can monitor and provide protection over one line, two lines, or all three lines (Fig. 1) depending on the status of the circuit breakers located at that busbar, and with appropriate re-configuration of the network data via the admittance matrix.

For accurate operation of the algorithm, as already alluded to above, the line parameters need to be precise. However, the available data may poorly reflect the actual line parameters. The line parameters may also vary with the environmental conditions [37]. It can also be deduced from14that the sensitivity terms are affected by frequency deviations in various ways, e.g. (1) Frequency deviations impact the performance of the PMU in terms of accuracy of the voltage phasor measurements and reporting latency [34]. However, adaptive filtering techniques reported in [34,37] can extract exact phasors in the presence of frequency deviation and harmonics. (2) The line admittances are also influenced by frequency deviations. Line parameter estimation using state estimation (SE) algorithms are reported in the literature [38]. The estimation algorithms based on PMU measurements, such as reported in [37,39] are especially valid for the protection algorithm reported in this paper because the system already uses PMU data as the basis for its functionality. Incorporation of the adaptive filtering and line parameter estimation algorithms give rise to the adaptive form of the algorithm. However, this adaptive form is not implemented in this paper. This paper, however, shows that the proposed protection algorithm works correctly to detect faults using power differential and sensitivity calculations and assumes that all the network parameters are assessed correctly.

4.5. Fault detection and identification logic

The fault detection and identification logic of the proposed algorithm is illustrated in Fig. 6. Communication plays a major role in identifying the actual faulted feeder in the network. A Fault Detection and Identification (FDI) flag is defined for each relay. The FDI flag is asserted to logic '1' if a fault is detected at a node when FD-Indices $C_{k,P}$

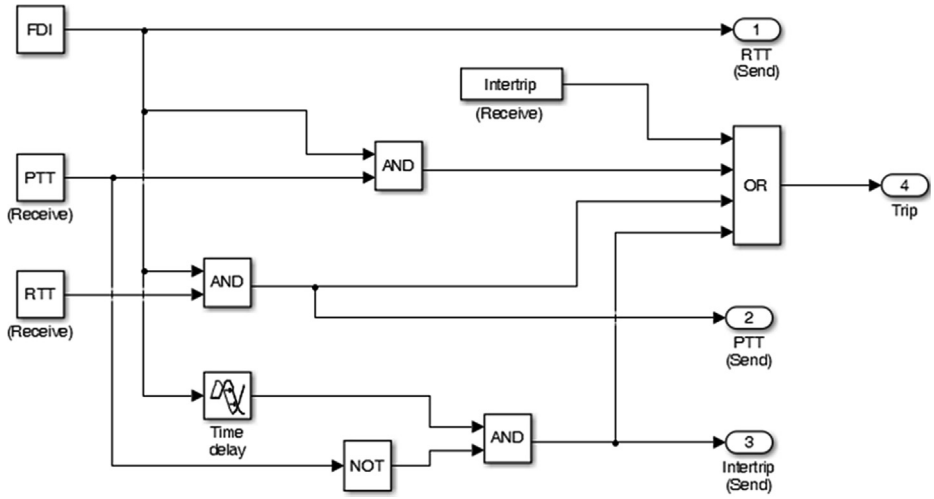

Fig. 6. Logic diagram.

and/or $C_{k,F}$, above threshold appear. The FD-Indices are generated when fault occurs anywhere within the protected zone. The logic for the correct identification and isolation of the fault is as follows.

When a fault is detected by an IED at a node (i.e., FDI = 1), the IED sends a Request To Trip (RTT) signal to the IEDs at the remote ends of the feeders terminating at that node. If one of the Remote IED Devices (RD) has also detected a fault it sends a Permission To Trip (PTT) signal back to the Primary Device (PD) that sent the RTT, at the same time tripping its local CB on the feeder linking to the PD. On receipt of the PTT signal the PD also trips its local CB on the feeder linking to the RD. If no PTT is received from any of the other RDs at the remote ends of the remaining feeders, then those feeders are not tripped. In this way only the faulted feeder is tripped. Where none of the RDs has detected a fault, which is the case when the fault is on the PD node itself, then on expiry of a time delay (during which the PD expects to receive a PTT from one of the RDs), the PD trips all the local CBs to clear the busbar fault.

If a fault occurs but the communication link has failed between the PD and one of the RDs, then the RTT or PTT signals cannot be sent or received to/from the concerned RD. Since none of the remaining RDs has detected a fault, then on expiry of the time delay, the PD trips all the local CBs and sends inter-trip signals to those RDs with which it has active communication links. All the feeders terminating at the PD are tripped. The CB at the remote end of the faulted feeder, however, is still closed as far as the PD is concerned. Now, the remote RD is also a PD as far as its location is concerned. So its action replicates that of the other PD at the remote end. On expiry of the time delay, the 'remote' PD will trip all the 'local' CBs and sends inter-trip signals to those RDs with which it has active communication links. Those feeders terminating at the 'remote' PD are also tripped. Hence, the total sum of all feeders terminating at the two 'PDs' are tripped. Failure of a communication link thus results in wider outage but if the fault is temporary, reclosure is successful and supply is quickly restored.

5. Modelling of the proposed relay type

A protection relay type based on the proposed algorithm was modelled in DigSilent Powerfactory. The relay model and the associated measurement devices are installed at all the nodes of the test network in order to demonstrate its functionality under different scenarios.

The functional blocks of a relay may be represented as shown in Fig. 7, irrespective of implementation technology. The various blocks, as implemented in the new relay type, are described below.

5.1. Input and signal conditioning

The protection algorithm is voltage-based and requires measurement of the voltage magnitude and phase using PMUs located at each node. The modelling presented in this paper uses the PowerFactory in-built phase measurement device (*ElmPhi*) to provide the absolute phase angle of voltage at a node referenced to the slack bus. The voltage magnitude is provided by the voltage measurement device (*StaVmea*). The PowerFactory in-built PQ measurement devices (*StaPqmea*) were used for the measurement of the net power flow in the BAP segment (which gives the power flow at node *k*). The PQ measurement devices are installed at the extremities of the unit BAP segment to effectively check the input-output power balance in the segment. Detailed information on relay modelling in PowerFactory can be found in [40].

5.2. Decision making

The decision making stage runs the proposed algorithm. As already explained in Section 4, the decision making uses the FD-Indices $C_{k,P}$ and $C_{k,F}$. The decision is manifested in the status of the FDI flag at each node. The fault detection logic is described in Section 4.3, and is programmed in *PowerFactory* using the Digsilent Simulation Language (DSL).

5.3. Scheme logic

The output stage basically implements the logic represented in Fig. 6. The appropriate CBs are identified and tripped to isolate and clear the fault when the FDI flag is asserted at one or more nodes. The logic represented in Fig. 6 trips the CB on a particular feeder along which a fault has been detected. This logic must be replicated for all the CBs at a particular node, depending on the number of feeders terminating at that node. Thus the relay based on this algorithm will have trip outputs that equal the number of CBs at the particular node in the network.

5.4. Composite frame of the relay

The complete composite frame of the new type relay is shown in Fig. 8. The frame shows the interconnections between the measurement devices, the measurement modules, the relay algorithm module and the scheme logic module, together with the signal flows between them. The measurement module represents a simple mathematical formulation that helps to differentiate between the various instances of bus measurement outputs. The number of inputs to the relay depends on the

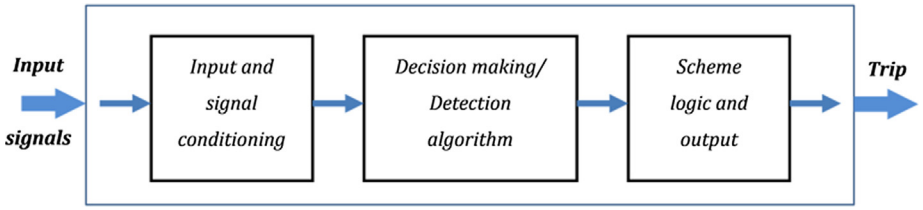

Fig. 7. Relay functional blocks.

number of feeders terminating at the node at which the relay is installed. The frame shown in Fig. 8 is for a relay for installation at, for example, node 3 of the test network in Fig. 2. The relay requires voltage measurements from nodes 2, 4 and 8 in addition to the local voltage measurements at node 3. The nodes within each BAP zone are renumbered 1 … n, where n is the total number of nodes in the zone (and is equal to 4 for Zone3). However, as already discussed in Section 4.4 the protection algorithm can be reconfigured to match the number of feeders terminating at node k.

The relay models are installed at each node in the test system and customized to receive input signals from the correct measurement devices (in the respective zone) and also customized to trip the associated CBs at the particular node.

6. Results and discussion

The relay models and the associated measurement devices are installed at the nodes of the MV test network of Fig. 2. The relays are configured to match the number of feeders terminating at each node.

6.1. Relay pick-up threshold settings

The $C_{k,P}$ and $C_{k,F}$ FD-Indices generated by connection of load (ΔP_{Load}) establish, at each node, the relay pick-up threshold settings that must be applied to the relay in order to prevent erroneous tripping when load is connected or disconnected. Above this threshold fault is indicated. Preliminary power differential and sensitivity calculations need to be performed to determine the threshold values. The results of this study are shown in Table 1 for both the grid-connected and isolated modes of operation. FD-Indices of similar magnitudes are obtained in

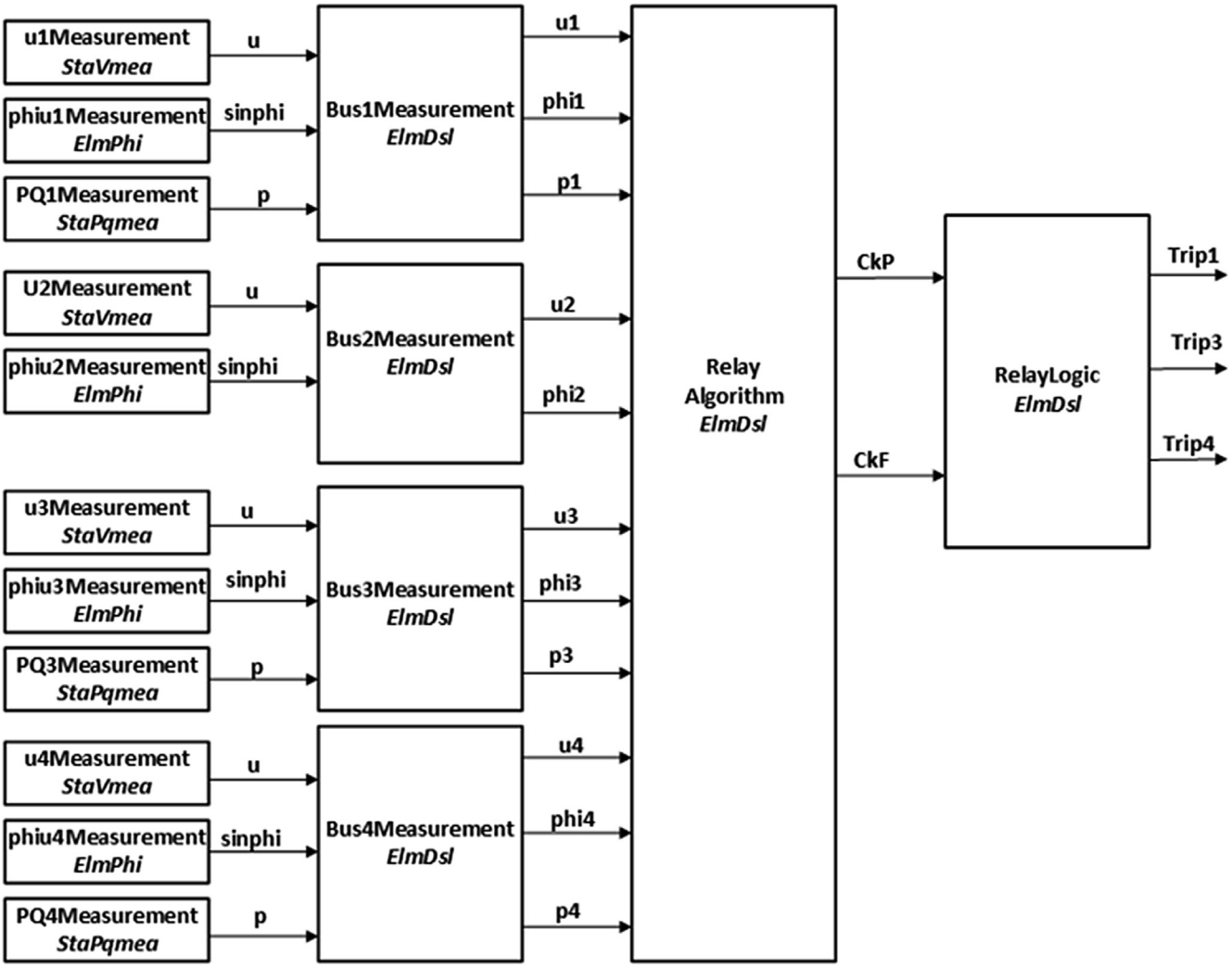

Fig. 8. Composite frame of the new relay type in PowerFactory. (Relay is located at node $k = 2$).

Table 1
FD-Indices generated by connection of load at all the nodes.

	Isolated		Grid-connected	
Node	$C_{k,P}$	$C_{k,F}$	$C_{k,P}$	$C_{k,F}$
1	0.63	0.52	0.89	0.68
2	0.00	0.00	0.00	0.00
3	0.70	0.41	0.70	0.62
4	0.60	0.41	0.60	0.47
5	1.01	1.07	1.01	1.19
6	0.76	0.60	0.76	0.67
7	0.11	0.01	0.11	0.02
8	0.82	0.39	0.82	0.64
9	0.80	0.81	0.80	0.90
10	0.76	0.61	0.76	0.68
11	0.46	0.22	0.46	0.24
12	0.16	0.03	0.16	0.04
13	0.05	0.01	0.05	0.00
14	0.75	0.50	0.75	0.75

Table 2
FD-Indices generated by three-phase fault at selected nodes with fault resistance $R_F = 1\ \Omega$.

	Isolated		Grid-connected	
Node	$C_{k,P}$	$C_{k,F}$	$C_{k,P}$	$C_{k,F}$
2	25.49	3585.39	277.05	48304.33
3	22.79	2510.72	103.96	15538.22
5	21.74	2468.31	86.52	13581.96
6	18.45	1770.68	67.70	9077.58
9	20.89	2120.64	87.08	11718.08
11	20.26	1986.15	81.44	10764.30
13	36.64	7040.19	191.96	47723.70
14	31.94	5255.92	134.30	29750.99

the two cases. No load is connected at node 2, hence the zero magnitude FD-Indices.

6.2. Fault detection

Faults generate FD-Indices that are significantly larger than those due to connection of load, as shown in Table 2 for three-phase faults at a selected number of nodes in the network. The indices in the grid connected mode are larger than in the isolated case. FD-Indices of similar magnitudes are also obtained for single phase-to-ground and phase-to-phase faults.

Table 3 shows the magnitude of the FD-Indices generated (at all nodes) for three-phase faults of different resistances at the mid-point of Feeder 3–8. It can be seen that positive FD-Indices are only generated at nodes 3 and 8. The FD-Indices at all other nodes are zero or negative; actually less than the pick-up thresholds established in Table 1. Using peer-to-peer communications, the IEDs at nodes 3 and 8 identify the fault to be on the feeder linking the two nodes and act appropriately to trip the CBs on Feeder 3–8. Fault detection and identification is possible over a wide range of fault resistances as illustrated by the results in Tables 3 for fault resistances of 1 Ω, 33 Ω and 330 Ω, respectively. However, fault detection becomes difficult at higher fault resistances due to the reduced magnitude of the fault indices.

Table 4 shows the magnitude of the FD-Indices generated (at all nodes) for single-phase to earth faults of different resistances at the mid-point of Feeder 9–10. Positive FD-Indices generated at nodes 9 and 10 enable the respective IEDs to detect the fault and trip the appropriate CBs. The fault indices generated for a phase-to-phase fault are shown in Table 5 for a fault along Feeder 5–6. It is seen that positive indices are recorded at nodes 5 and 6 only. On the healthy phase, very small or insignificant fault indices below pick-up threshold are generated, as shown in Table 6.

6.3. Fault detection range

The $C_{k,F}$ indices generated at node 5 are given in Table 7 for single phase to earth fault of various resistances occurring at different distances along Feeder 5–6, measured from node 5. Distances of 0% and 100% indicate fault at node 5 or 6, respectively. It can be seen that detectable fault indices are generated for faults occurring at distances up to 95% from the relay location. However, faults at the remote node (100% distance) cannot be detected by the relay at node 5. This is consistent with the principle of the protection algorithm, that the protection must see faults only within its BAP zone (that includes a busbar and all feeders terminating at that busbar). The relay cannot see faults at the remote busbar because that busbar belongs to the BAP zone of the remote relay. This fault is therefore detected by the remote IED at node 6.

As can be seen, faults close-up (within 5% range) to a node are also not seen by the remote IED. Since a busbar and close-up fault cannot be differentiated, inter-trip signals must be sent to trip the remote CBs of that zone, effectively isolating the entire zone, as explained in Section 4.5. However, successful re-closure may ensure quick restoration of supplies.

The results in Tables 1–7 clearly demonstrate the principle on which the protection algorithm is based: FD-Indices based on power

Table 3
FD-Indices generated at all nodes for a three-phase fault at mid-point of Feeder 3–8 ($R_F = 1\ \Omega$).

			Grid connected						Grid isolated			
	$R_F = 1\ \Omega$		$R_F = 33\ \Omega$		$R_F = 330\ \Omega$		$R_F = 1\ \Omega$		$R_F = 33\ \Omega$		$R_F = 330\ \Omega$	
Node	CkP	CkF	CkP	CkF	CkP	CkF	CkP	CkF	CkP	CkF	CkP	CkF
1	−89.31	−9701.07	−11.00	−99.31	−1.17	−1.07	−28.96	−284.24	−2.46	−6.85	−0.17	−0.03
2	0.00	0.00	0.00	0.00	0.00	0.00	0.00	0.00	0.00	0.00	0.00	0.00
3	48.48	2534.86	12.18	140.11	1.32	1.72	10.58	490.48	10.65	108.15	1.16	1.33
4	−38.02	−995.45	−49.85	−73.18	−48.98	−9.17	–32.00	−1164.15	−54.36	−271.70	−49.52	–32.73
5	−0.89	−0.48	−0.08	−0.01	−0.01	0.00	−0.98	−0.36	−0.08	−0.01	−0.01	0.00
6	−0.67	−0.27	−0.06	0.00	−0.01	0.00	−0.74	−0.20	−0.06	0.00	0.00	0.00
7	−0.09	−0.01	−0.01	0.00	0.00	0.00	−0.10	0.00	−0.01	0.00	0.00	0.00
8	63.26	16070.05	11.94	412.01	1.28	4.36	34.34	5537.68	5.91	90.98	0.54	1.89
9	−0.70	−0.37	−0.07	−0.01	−0.01	0.00	−0.77	−0.27	−0.06	−0.01	0.00	0.00
10	−0.66	−0.28	−0.06	0.00	−0.01	0.00	−0.73	−0.21	−0.06	0.00	0.00	0.00
11	−0.40	−0.10	−0.04	0.00	0.00	0.00	−0.44	−0.07	−0.04	0.00	0.00	0.00
12	−62.27	−4762.33	−8.28	−45.14	−0.89	−0.48	−24.66	−96.72	−7.30	−37.87	−0.74	−0.45
13	−0.03	−0.08	0.00	0.00	0.00	0.00	−0.04	−0.02	0.00	0.00	0.00	0.00
14	−0.60	−0.23	−0.05	−0.01	0.00	0.00	−0.71	−0.03	−0.04	−0.01	0.00	0.00

Table 4
FD-Indices generated at all nodes for a single-phase to ground fault at mid-point of Feeder 9–10 (R_F = 1 Ω).

	Grid connected						Grid isolated					
	R_F = 1 Ω		R_F = 33 Ω		R_F = 330 Ω		R_F = 1 Ω		R_F = 33 Ω		R_F = 330 Ω	
Node	CkP	CkF	CkP	CkF	CkP	CkF	CkP	CkF	CkP	CkF	CkP	CkF
1	−3.97	−69.80	−0.41	−0.06	−0.04	0.00	−83.61	−7062.21	−16.60	−211.01	−1.81	−2.31
2	0.00	0.00	0.00	0.00	0.00	0.00	0.00	0.00	0.00	0.00	0.00	0.00
3	−0.60	−1.93	−0.06	−0.01	−0.01	0.00	−0.60	−1.09	−0.06	−0.03	−0.01	0.00
4	−12.26	−329.66	−0.70	−0.85	−0.09	−0.01	−36.16	−1250.77	−53.31	−40.48	−50.47	−8.09
5	−0.89	−0.48	−0.09	−0.01	−0.01	0.00	−0.90	−0.42	−0.11	−0.02	−0.01	0.00
6	−0.67	−0.27	−0.07	−0.01	−0.01	0.00	−0.68	−0.24	−0.08	−0.01	−0.01	0.00
7	−0.09	−0.01	−0.01	0.00	0.00	0.00	−0.09	−0.01	−0.01	0.00	0.00	0.00
8	−9.32	−2561.15	−0.61	−15.52	−0.08	−0.19	−10.75	−2096.45	−1.72	−59.46	−0.24	−0.65
9	39.80	2016.94	11.64	128.29	1.27	1.61	24.12	1693.61	15.89	175.65	1.82	2.47
10	38.71	2099.63	11.65	128.49	1.28	1.62	23.76	1705.59	15.89	175.18	1.82	2.47
11	−0.41	−0.23	−0.04	0.00	0.00	0.00	−0.42	−1.40	−0.05	−0.01	0.00	0.00
12	−0.36	−3.43	−0.03	0.00	0.00	0.00	−19.17	−340.50	−6.22	−18.74	−0.71	−0.19
13	−0.03	−0.06	0.00	0.00	0.00	0.00	−0.04	−0.12	0.00	0.00	0.00	0.00
14	−0.60	−0.16	−0.05	−0.01	−0.01	0.00	−0.64	−3.50	−0.07	−0.02	−0.01	0.00

Table 5
FD-Indices generated by phase-phase fault at mid-point of Feeder 5–6 (R_F = 0.1 Ω).

	Isolated		Grid-connected	
Node	$C_{k,P}$	$C_{k,F}$	$C_{k,P}$	$C_{k,F}$
1	−74.81	−5199.89	−3.66	−112.50
2	0.00	0.00	0.00	0.00
3	−0.41	−6.56	−0.47	−7.23
4	−44.72	−486.27	−7.30	−85.19
5	36.20	116.87	50.96	77.35
6	33.38	104.77	45.03	17.31
7	−0.07	−0.05	−0.08	−0.10
8	−5.85	−647.38	−6.80	−1392.55
9	−0.48	−0.26	−0.54	−0.33
10	−0.46	−0.19	−0.51	−0.26
11	−0.28	−0.07	−0.31	−0.10
12	−5.18	−21.34	−0.25	−6.45
13	−0.03	0.00	−0.02	−0.26
14	−0.46	−0.19	−0.46	−3.31

Table 6
FD-Indices generated on the healthy phase for a phase-phase fault at mid-point of Feeder 5–6 (R_F = 0.1 Ω).

	Isolated		Grid-connected	
Node	$C_{k,P}$	$C_{k,F}$	$C_{k,P}$	$C_{k,F}$
5	0.04	0.02	0.01	0.00
6	0.03	0.01	0.00	0.00

differential and sensitivity calculations (using voltage measurements only) can be used to distinguish a fault condition from a normal operational condition without any knowledge of the contributions of the DERs to the fault current. The protection algorithm is 'differential'. That is, the relay sees a fault within its zone only. When an external fault occurs, FD-Indices which are zero or negative are generated but these serve to improve the stability of the relay to external faults since magnitude of these indices are actually driven negative relative to the pick-up threshold setting.

6.4. Performance of the proposed relay type

Fig. 9 illustrates the operation of the relay at node 5 for a single-phase to ground fault (of 1 Ω resistance) on the feeder linking to node 6. The fault occurs at 0.1 s. It is seen that when the fault occurs the FD-Indices ($C_{k,P}$ and $C_{k,F}$) change state from zero to some positive magnitude after the fault is detected. The FDI signal is immediately asserted to '1' and RTT signals are immediately sent to the RDs at the neighbouring nodes 4 and 6.

A similar set of signals are generated by the relay at node 6 and in this case RTT signals are sent to the RDs at its neighbouring nodes 5 and 7. Relay at node 5 then receives a PTT signal from the relay at node 6; similarly relay at node 6 received a PTT signal from relay at node 5. The fault is now located to be on Feeder 5–6. Trip signal *Trip3* of relay at node 5 is asserted leading to tripping of CB linking to node 6. Similarly, the appropriate trip signal of relay at node 6 is asserted leading to tripping of CB linking to node 5. The faulted feeder is thus isolated.

Operation of the relay at node 5 for the same fault when the microgrid is isolated from the grid is shown in Fig. 10. FD-Indices $C_{k,P}$ and $C_{k,F}$ that are much larger than the pick-up thresholds are still generated. Similar results are obtained under a variety of fault types and fault resistances showing that the proposed relay type is able to detect and identify faults in a microgrid in both grid-connected and isolated modes of operation.

7. Conclusion

A relay type based on voltage measurements only was developed

Table 7
C_{kF} indices generated at Node 5 for a single-phase to ground fault at various points along Feeder 5–6.

	Grid connected						Grid isolated					
	Distance from Node 5						Distance from Node 5					
R_F	0%	25%	75%	95%	99%	100%	0%	25%	75%	95%	99%	100%
1	29658.94	9478.32	470.21	20.62	−0.91	−12.18	16780.14	5620.28	302.03	9.19	−4.45	−11.62
3	2316.65	655.93	13.00	0.90	0.01	−0.06	3397.02	1418.18	81.06	0.34	0.02	−0.54
33	793.40	443.25	47.06	1.41	0.02	−0.03	711.86	396.68	41.65	1.17	0.02	−0.04

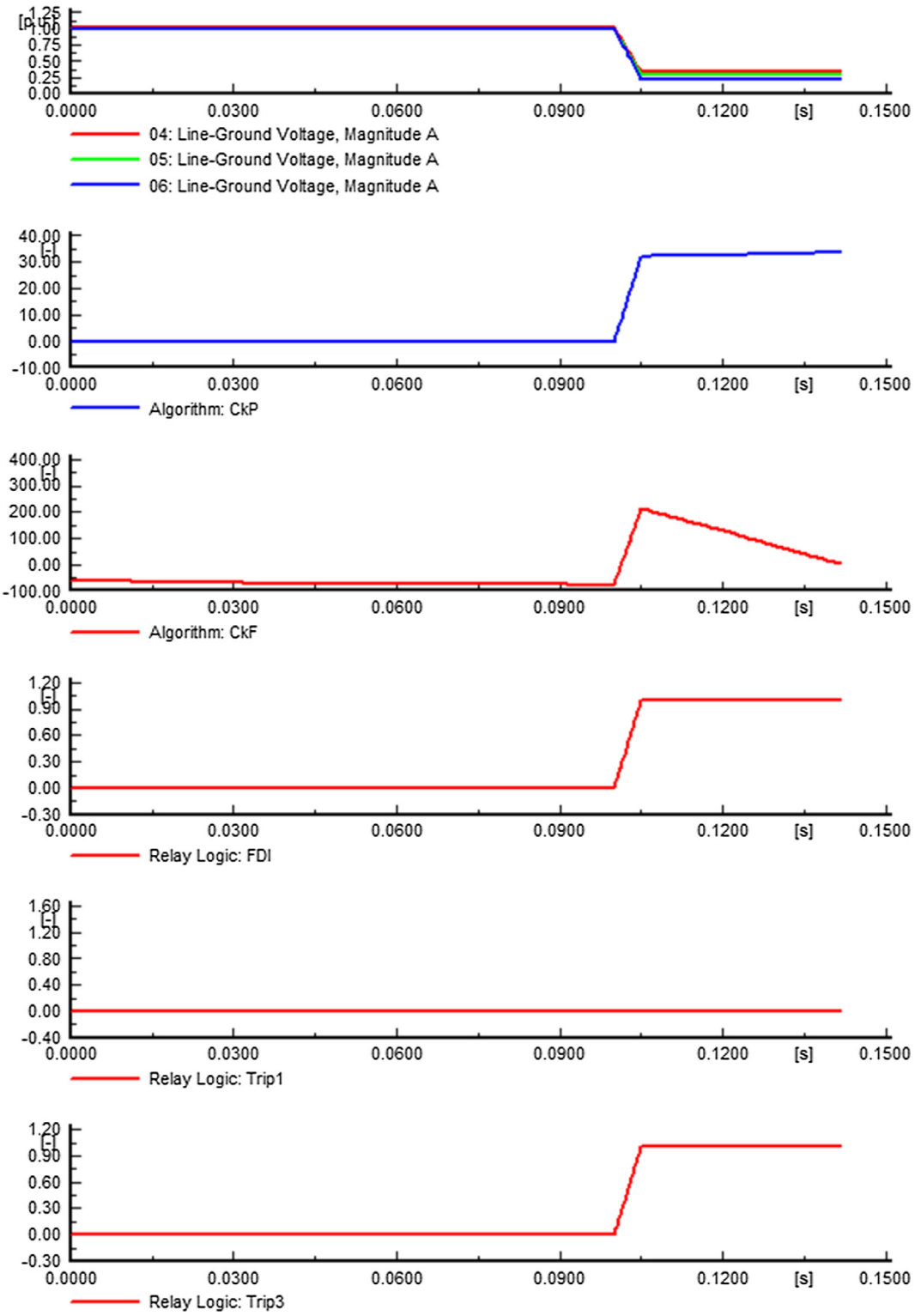

Fig. 9. Protection signals at node (Relay) 05 (with microgrid in grid-connected mode).

and modelled in Digsilent PowerFactory. The relay achieves its protection function through power differential and sensitivity calculations based on voltage measurements within a specified protection zone. The relay model and the associated measurement devices were installed at the nodes of a microgrid based on the CIGRE benchmark MV test network. The relay is shown to operate correctly and effectively to detect and identify all types of faults – single-phase or multi-phase - in the microgrid in both grid-connected and isolated modes of operation. It is applicable to microgrids with the simple radial or meshed topologies. Only one relay based on the proposed algorithm is required at a node.

CRediT authorship contribution statement

Patrick T. Manditereza: Conceptualization, Methodology, Investigation, Visualization, Writing - original draft. **Ramesh C. Bansal:** Writing - review & editing, Supervision.

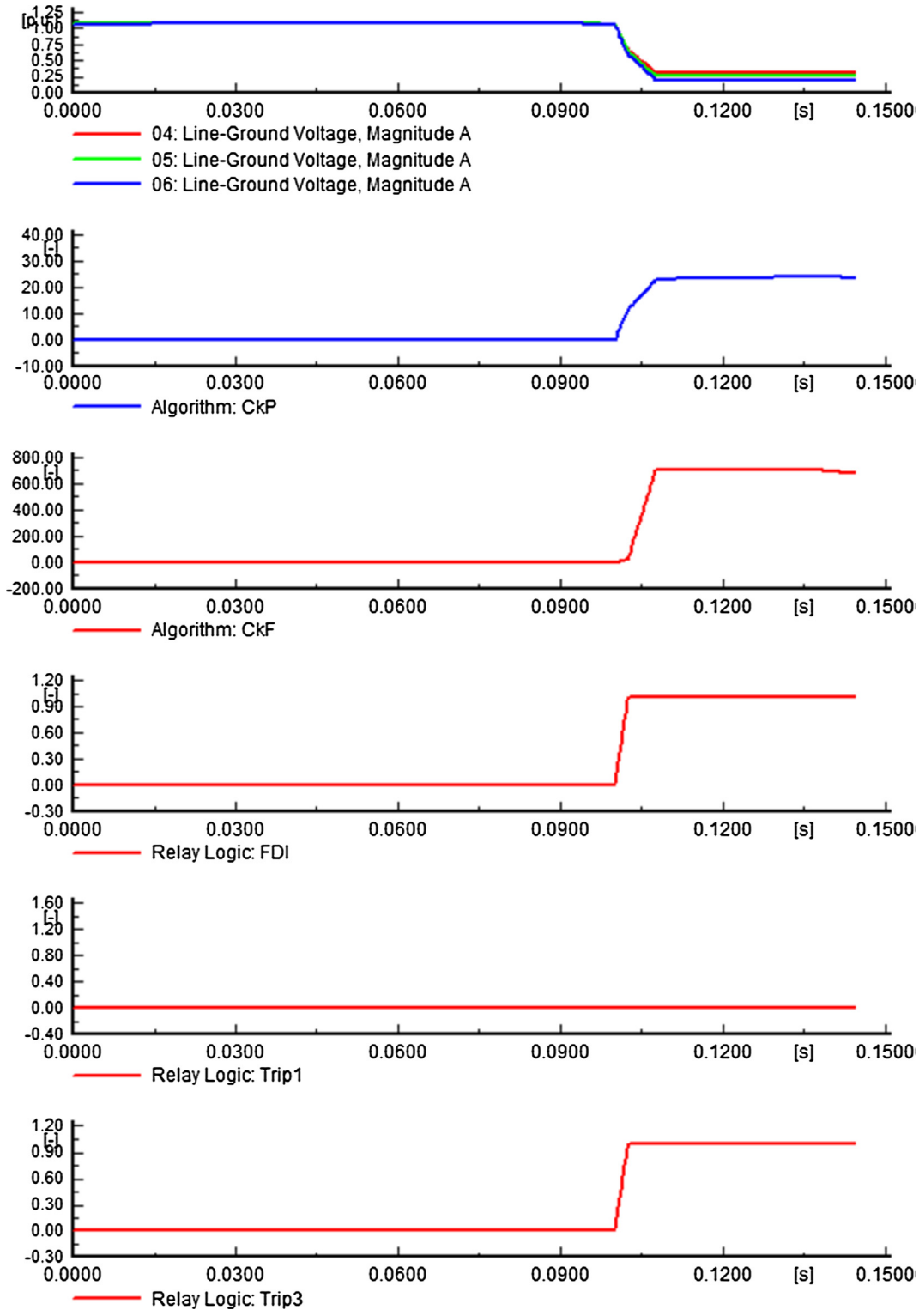

Fig. 10. Protection signals at node (Relay) 05 (with microgrid in isolated mode).

Declaration of Competing Interest

The authors declare that they have no known competing financial interests or personal relationships that could have appeared to influence the work reported in this paper.

References

[1] Mandiereza PT, Bansal RC. Renewable distributed generation: the hidden challenges – a review from the protection perspective. Renew Sustain Energy Reviews 2016;58:1457–65.
[2] Aguero JR, Khodaei A, Masiello R. The utility and grid of the future: challenges, needs, and trends. IEEE Power Energ Mag 2016;14(5):29–37.
[3] Mandiereza PT, Bansal RC. Introducing a new type of protection zone for the smart grid incorporating distributed generation. In: Proceedings of the IEEE PES International Conference on Innovative Smart Grid Technologies (ISGT), Singapore,

22–25 May 2018. p. 86–90.
[4] A. Hooshyar, R. Iravani, Microgrid protection, in: Proceedings of the IEEE, vol. 105, no. 7, July 2017. p. 1332–52.
[5] Hirscha A, Paraga Y, Guerrerob J. Microgrids: a review of technologies, key drivers, and outstanding issues. Renew Sustain Energy Rev 2018;90:402–11.
[6] Blaabjerg F, Yang Y, Yang D, Wang X. Distributed power-generation systems and protection. In: Proceedings of the IEEE 2017;105(7):1311–31.
[7] Zarei SF, Parniani M. A comprehensive digital protection scheme for low-voltage microgrids with inverter-based and conventional distributed generations. IEEE Trans Power Delivery 2017;32(1):441–52.
[8] Hooshyar A, Iravani R. A new directional element for microgrid protection. IEEE Trans Smart Grid 2018;9(6):6862–76.
[9] Muda H, Jena P. Superimposed adaptive sequence current based microgrid protection: a new technique. IEEE Trans Power Delivery 2017;32(2):757–67.
[10] Liu X, Shahidehpour M, Li Z, Liu X, Cao Y, Tian Wei. Protection scheme for loop-based microgrids. IEEE Transactions on Smart Grid 2017;8(3):1340–9.
[11] Ustun TS, Khan RH. Multiterminal hybrid protection of microgrids over wireless communications network. IEEE Trans Smart Grid 2015;6(5):2493–500.
[12] Oureilidis KO, Demoulias CS. A fault clearing method in converter-dominated microgrids with conventional protection means. IEEE Trans Power Electron 2016;31(6):4628–40.
[13] Orji U, Schantz C, Leeb SB, Kirtley JL, Sievenpiper B, Gerhard K, et al. Adaptive zonal protection for ring microgrids. IEEE Trans Smat Grid 2017;8(4):1843–51.
[14] Sharaf HM, Zeineldin HH, El-Saadany E. Protection coordination for microgrids with grid-connected and islanded capabilities using communication assisted dual setting directional overcurrent relays. IEEE Trans Smart Grid 2018;9(1):143–51.
[15] Cintuglu MH, Ma T, Mohammed OA. Protection of autonomous microgrids using agent-based distributed communication. IEEE Trans. Power Delivery 2017;32(1):351–60.
[16] Chen Z, Pei X, Yang M, Peng L, Shi P. A novel protection scheme for inverter-interfaced microgrid (IIM) operated in islanded mode. IEEE Trans Power Electron 2018;33(9):7684–97.
[17] Manditereza PT, Bansal RC. Review of technical issues influencing the decoupling DG converter design from the distribution system protection strategy. Renew Power Gener 2018;12(10):1091–100.
[18] Manditereza PT, Bansal RC. Fault detection and location algorithm for DG integrated distribution systems. IET J Eng 2018;2018(15):1286–90.
[19] Al-Nasseri H, Redfern MA. Harmonics content based protection scheme for microgrids dominated by solid state converters. In: 12th Int. Middle-East Power System Conf. (MEPCON), Aswan, Egypt, March 2008. p. 50–6.
[20] Al-Nasseri H, Redfern MA, Li F. Voltage based protection for microgrids microgrids. In: IEEE Power Engineering Society General Meeting, Montreal, Canada, June 2006. p. 1–5.
[21] Tumilty RM, Brucoli M, Burt GM, Green TC. Approaches to network protection for inverter dominated electrical distribution systems. In: 3rd IET International Conference on Power Electronics, Machines and Drives, Dublin, Ireland, April 2006. p. 622–6.
[22] Affijulla S, Tripathy P. Development of phasor estimation algorithm for P-Class PMU suitable in protection applications. IEEE Trans Smart Grid 2018;9(2):1250–60.
[23] Biswal M, Brahma SM, Cao Huiping. Supervisory protection and automated event diagnosis using PMU data. IEEE Trans Power Del 2016;31(4):1855–63.
[24] Hatziargyriou N. Microgrids: Architectures and Control. 1st ed. N. Hatziargyriou, Ed. Chichester, West Sussex, UK: John Wiley & Sons; 2014.
[25] Fu Q, Nasiri A, Solanki A, Bani-Ahmed A, Weber L, Bhavaraju V. Microgrids: architectures, controls, protection, and demonstration. Electr Power Compon Syst 2015;43(12):1453–65.
[26] Skok S, Ivankovic I, Sturlic I, Ugarkovic K. Microgrid monitoring protection and control based on synchronized measurements. In: CIGRE SC D2 International Colloquium, Moscow, Russia, 20–22 September 2017. p. 1–7.
[27] Barella R, Nguyen D, Winter R, Lu KT, Wallace S, Zhao X, Cotilla-Sanchez E. A sensitivity study of PMU-based fault detection on smart grid. In: International Conference on Smart Cities and Green ICT Systems (SMARTGREENS), Lisbon, 20–22 May 2015. p. 1–8.
[28] Almas MS, Vanfretti L. A method exploiting direct communication between phasor measurement units for power system wide-area protection and control algorithms. MethodsX 2017;4:346–59.
[29] Almas MS, Vanfrett L. RT-HIL implementation of the hybrid synchrophasorand GOOSE-based passive islanding schemes. IEEE Trans Power Del 2016;31(3):1299–309.
[30] Almas M, Vanfretti L. A hybrid synchrophasor and GOOSE-based power system synchronization scheme. IEEE Access 2016;4:4659–68.
[31] Jamei M, Stewart E, Peisert S, Scaglione A, McParland C, Roberts C, McEachern A. Micro synchrophasor-based intrusion detection in automated distribution systems: toward critical infrastructure security. IEEE Internet Computing 2016;20(5):18–27.
[32] von Meier A, Stewart E, McEachern A, Andersen M, Mehrmanesh L. Precision micro-synchrophasors for distribution systems: a summary of applications. IEEE Trans Smart Grid 2017;8(6):2926–36.
[33] Elbana MS, Abbasy N, Meghed A. μPMU-based smart adaptive protection scheme for microgrids. Modern Power Syst Clean Energy 2019;7(4):887–98.
[34] Blair SM, Syed MH, Roscoe AJ, Burt GM, Braun JP. Measurement and analysis of PMU reporting latency for smart grid protection and control applications. IEEE Access 2019;7:48689–98.
[35] Cigre. Benchmark systems for network integration of renewable and distributed energy resources. Task Force C6.04.02 2014.
[36] Manditereza PT, Bansal RC. Multi-agent based distributed voltage control algorithm for smart grid applications. Electr Power Compon Syst 2016;44(20):2352–63.
[37] Jiang JA, Lin YH, Yang JZ, Too TM, Liu CW. An adaptive PMU based fault detection/location technique for transmission lines—Part II: PMU implementation and performance evaluation. IEEE Trans Power Delivery 2000;15(4):1136–46.
[38] Neshvad S, Margossian H, Sachau J. Topology and parameter estimation in power systems through inverter-based broadband stimulations. IET Gener Transm Distrib 2016;10(7):1710–9.
[39] Li J, Wang X, Ren X, Zhang Y, Zhang F. Augmented state estimation method for fault location based on on-line parameter identification of PMU measurement data. In: IEEE 2nd International Electrical and Energy Conference (CIEEC), Beijing, China, 4–6 November, 2018. p. 105.
[40] DIgSILENT GmbH. (May 2015) DIgSILENT PowerFactory. User Manual.